Energy dependence of J/ψ absorption in proton-nucleus collisions

Carlos Lourenço
CERN-PH, CH-1211 Geneva 23, *carlos.lourenco@cern.ch*

Ramona Vogt
LLNL, Livermore, CA 94550, USA, *vogt2@llnl.gov*
and University of California, Davis, CA, USA

Hermine K. Wöhri
LIP, Lisbon, Portugal, *hermine.woehri@cern.ch*

Abstract

Charmonium states are expected to be considerably suppressed in the case of quark-gluon plasma formation in high-energy heavy-ion collisions. However, a robust identification of suppression patterns as signatures of a deconfined QCD medium requires a detailed understanding of the "normal nuclear absorption" already present in proton-nucleus collisions, where the charmonium production cross sections increase less than linearly with the number of target nucleons. We analyse the J/ψ production cross sections measured in proton-nucleus collisions in fixed target experiments, with proton beam energies from 200 to 920 GeV, and in d-Au collisions at RHIC, at $\sqrt{s_{NN}} = 200$ GeV, in the framework of the Glauber formalism, using several sets of parton distributions with and without nuclear modifications. The results reveal a significant dependence of the "absorption cross section" on the kinematics of the J/ψ and on the collision energy. Extrapolating the observed patterns we derive the level of absorption expected at $E_{\rm lab} = 158$ GeV, the energy at which the heavy-ion data sets were collected at the CERN SPS.

Keywords: J/ψ absorption, cold nuclear matter effects

Submitted to JHEP

Contents

1 Introduction

According to lattice QCD calculations [1], when hadronic matter reaches sufficiently high energy densities it should undergo a phase transition to a "plasma" of deconfined quarks and gluons (the QGP phase). Considerable efforts are currently being invested in the study of high-energy heavy-ion collisions to reveal the existence of this phase transition and to study the properties of the new phase in view of improving our understanding of confinement, a crucial feature of QCD. The production yields of the quarkonium states should be considerably suppressed by "colour screening" if a QCD medium with deconfined quarks and gluons is formed in high-energy heavy-ion collisions [2]. However, already in proton-nucleus collisions the charmonium production cross sections increase less than linearly with the number of binary nucleon-nucleon collisions. This "normal nuclear absorption" needs to be well understood so that a robust baseline reference can be established, with respect to which we can clearly and unambiguously identify the signals of "new physics" specific to the high density QCD medium.

So far, the studies of the J/ψ suppression patterns determined by the NA50 and NA60 experiments at the SPS, from data collected with Pb and In ion beams of 158 GeV per nucleon, use a baseline reference established on the basis of proton-nucleus measurements performed at 400 and 450 GeV, assuming that the energy dependencies of the initial and final state "normal nuclear effects", if any, can be neglected. It is important to verify if this simple assumption is supported or not by existing experimental evidence, looking at the results reported by experiments made at different energies, complementing and placing in a broader context the results to be obtained by NA60 from proton-nucleus measurements made at 158 GeV.

In this paper we present a detailed study of some "cold nuclear matter effects" affecting charmonium production in proton-nucleus collisions, as well as their energy dependence. Section 2 gives a brief historical motivation. Section 3 describes the basic framework of our study: how the charmonium production cross sections are calculated and how the absorption of the charmonium states in the nuclear matter is evaluated. Comparing our calculations to the midrapidity J/ψ production cross sections measured in proton-nucleus collisions by NA3 (200 GeV), NA50 (400/450 GeV), E866 (800 GeV) and HERA-B (920 GeV), presented in Section 4, we observe a significant energy dependence of $\sigma_{\text{abs}}^{J/\psi}$ in this energy range. Simple parametrisations of this energy dependence lead to J/ψ normal nuclear absorption rates at the SPS heavy-ion energy, $E_{\text{lab}} = 158$ GeV, significantly larger than at higher energies, as presented and discussed in Section 5.

2 Brief historical motivation

The NA50 experiment at the CERN-SPS made a detailed study of J/ψ and ψ' production in fixed-target proton-nucleus collisions with incident protons of 400 and 450 GeV, employing six different nuclear targets (Be, Al, Cu, Ag, W and Pb) [3, 4]. Comparing

1

the production cross sections measured at 400 GeV, for instance, to calculations based on the Glauber formalism (neglecting nuclear modifications of the parton densities), the J/ψ "absorption cross section" was determined to be $\sigma_{\text{abs}}^{\text{J}/\psi} = 4.6 \pm 0.6$ mb [3]. A similar value, $\sigma_{\text{abs}}^{\text{J}/\psi} = 4.2 \pm 0.5$ mb, is extracted from a global fit to the 400 and 450 GeV J/ψ / DY cross-section *ratios*, where Drell-Yan dimuons are used as reference. This value has been used by NA50 [5] and NA60 [6] in the studies of the SPS heavy-ion data, collected at 158 GeV, assuming that the energy dependencies of the initial and final state "normal nuclear effects", if any, can be neglected.

An attempt was made [7] to check the reliability of this assumption, exploring the centrality dependence of the J/ψ / DY cross-section ratio measured by the NA38 experiment in S-U collisions at 200 GeV per nucleon. This study gave $\sigma_{\text{abs}}^{\text{J}/\psi} = 7.1 \pm 2.8$ mb, a value larger than the one derived from the higher energy data. However, this result is not satisfactory given the large uncertainty in the value of $\sigma_{\text{abs}}^{\text{J}/\psi}$ and the need to assume that there are no additional nuclear effects between the proton-nucleus and the S-U collision systems. We know, in particular, that the ψ' state is considerably more suppressed in S-U than in p-A collisions [8], and we should not assume that the J/ψ state is insensitive to the additional mechanisms of ψ' absorption.

Whether or not charmonium absorption depends on the collision energy still remains an open question. It is long known that E866, at FNAL, observed less J/ψ absorption at 800 GeV than seen by NA50 in the same $x_{\text{F}} \sim 0$ region. In terms of the very simple "α parametrisation",

$$\sigma_{\text{p A}} = \sigma_0 \times A^{\alpha} \quad , \tag{1}$$

NA50 reported $\alpha = 0.925 \pm 0.009$ at 400 GeV [3] while E866 obtained values around 0.95 [9].

At the other end of the energy scale, NA3 reported $\alpha \sim 0.94$ at $x_{\text{F}} \sim 0$ [10]. However, it has meanwhile been observed [11] that an absorption pattern generated using the Glauber framework, with a certain absorption cross section, leads to significantly different α values when the light target is Hydrogen (used by NA3) or Beryllium (used by E866). In other words, if NA3 had used Be as the light target, as did NA50 and E866, they would have obtained an α value around 0.92.

A global average of J/ψ absorption cross sections was recently reported [12], assuming that measurements collected with different beam particles and energies should reflect a single σ_{abs} value despite the observation that some of the values were mutually exclusive.

Knowing the crucial importance of the normal nuclear absorption baseline in the interpretation of the J/ψ suppression seen in the heavy-ion data and given that the charmonium absorption processes may very well depend on the collision energy [13], the NA60 experiment collected (in 2004) proton-nucleus collisions at 158 GeV, the energy of the Pb and In beams used by NA50 and NA60, with seven different nuclear targets (Be, Al, Cu, In, W, Pb and U). In addition, the PHENIX experiment at RHIC should soon report measurements of J/ψ absorption in $\sqrt{s_{NN}} = 200$ GeV d-Au collisions with much better accuracy than that available in Ref. [14]. These two sets

of results, obtained at very different energies, should help determine the existence of an energy dependence and significantly improve our understanding of the mechanisms causing the observed nuclear effects in charmonium production.

3 Basic elements of the calculations

This section describes the framework we have used to derive the J/ψ absorption cross sections. The calculations of the charmonium production cross sections are performed with the colour evaporation model (CEM) using several sets of parton distribution functions (PDFs). It should be emphasised, however, that our results are derived by studying how the production yields change from light to heavy targets and, therefore, are essentially insensitive to the specific production model and set of PDFs used. We performed calculations with "free proton" PDFs and also with PDFs modified by the nuclear environment, using several parametrisations of the nuclear modifications. The survival probability of the charmonium states traversing the nuclear matter was evaluated in the framework of the Glauber model.

3.1 Charmonium production cross sections

The charmonium production cross sections used in the studies reported in this paper were calculated using the colour evaporation model, described in detail in Ref. [15]. In the CEM, the production cross section of each charmonium state, $\tilde{\sigma}_i$, is assumed to be a constant fraction, F_i, of the total "closed charm" production cross section, calculated as the integral over the $c\bar{c}$ pair mass, m, of the $c\bar{c}$ cross section, from threshold, $2\,m_c$, to twice the mass of the lightest D meson, $2\,m_{\rm D} = 3.74$ GeV/c^2:

$$\frac{\mathrm{d}\tilde{\sigma}_i}{\mathrm{d}x_{\rm F}} = 2F_i \int_{2m_c}^{2m_{\rm D}} m\,\mathrm{d}m\,\frac{\mathrm{d}\sigma^{c\bar{c}}}{\mathrm{d}x_{\rm F}\,\mathrm{d}m^2} \quad , \tag{2}$$

where $x_{\rm F}$ is the $c\bar{c}$ longitudinal momentum fraction in the centre-of-mass frame of the two colliding hadrons.

At leading order in perturbative QCD, the $c\bar{c}$ hadroproduction cross section is given by the sum of two partonic contributions, gluon fusion (gg) and quark-antiquark annihilation ($q\bar{q}$), convoluted with the parton densities in the colliding hadrons, A and B [16]:

$$\begin{aligned}
\frac{\mathrm{d}\sigma^{c\bar{c}}}{\mathrm{d}x_{\rm F}\,\mathrm{d}m^2} &= \int_0^1 \mathrm{d}x_1\,\mathrm{d}x_2\,\delta(x_1 x_2 s_{_{NN}} - m^2)\,\delta(x_{\rm F} - x_1 + x_2) \\
&\qquad \left\{ f_g^A(x_1, m^2)\,f_g^B(x_2, m^2)\,\sigma_{gg}(m^2) + \right. \\
&\qquad \left. \sum_{q=u,d,s} [f_q^A(x_1,m^2)f_{\bar{q}}^B(x_2,m^2) + f_{\bar{q}}^A(x_1,m^2)f_q^B(x_2,m^2)]\sigma_{q\bar{q}}(m^2) \right\} \quad ,
\end{aligned} \tag{3}$$

3

where x_1 and x_2 are the momentum fractions carried by the two partons and $\sqrt{s_{NN}}$ is the centre-of-mass energy of the nucleon-nucleon collision. In our calculations we use leading order parton densities, evaluated at scale $m^2 = x_1\,x_2\,s_{NN}$.

A basic feature of the CEM is that $\mathrm{d}\sigma^{c\bar{c}}/\mathrm{d}x_\mathrm{F}\,\mathrm{d}m^2$ fully determines the energy and momentum dependencies of all the states. The hadronization of the $c\bar{c}$ pairs into charmonium states is nonperturbative, involving the emission of one or more soft gluons. Each state requires a different matrix element, condensed in the fractions F_i, calculated for each state: J/ψ, ψ', χ_{c_J}, etc. We note that $F_{\mathrm{J}/\psi}$ includes both direct J/ψ production and feed-down J/ψ production through χ_{c_J} radiative decays and ψ' hadronic decays.

3.2 Parton densities in the proton and in the nucleus

Deep inelastic scattering (DIS) and Drell-Yan measurements performed with nuclear targets have shown that the distributions of partons in nuclei are significantly modified relative to those in free protons. These nuclear modifications depend on the fraction of the total hadron momentum carried by the parton, x, on the momentum scale, Q^2, and on the mass number of the nucleus, A. While the mechanisms governing these modifications are not yet well understood, several groups have produced parametrisations, $S_i(A, x, Q^2)$, that convert the free-proton distributions for each parton i, $f_i^\mathrm{p}(x, Q^2)$, into nuclear ones, $f_i^A(x, Q^2)$, assuming factorisation:

$$f_i^A(x, Q^2) = S_i(A, x, Q^2) \times f_i^\mathrm{p}(x, Q^2) \quad . \tag{4}$$

Naturally, the nuclear modifications should depend on the spatial location of the nucleon inside the target, with the nucleons at the surface being less "shadowed" than those in the core of the nucleus [17]. This effect can be ignored in analyses of p-nucleus data samples integrated over collision centrality (as done in this work).

Figure 1 shows several parametrisations of the nuclear modification functions on a Pb nucleus for valence quarks (left) and gluons (right), calculated for the scale, Q, suitable for quarkonium production calculations with the MRST2001 LO [18] or CTEQ61L [19] PDF sets. Since the quark and antiquark distribution functions are directly probed by the nuclear DIS and Drell-Yan data, their nuclear effects are relatively well constrained and all parametrisations give similar results. The connection between the measurements and the nuclear *gluon* densities is much more indirect, however, relying on the scale dependence of the F_2 structure function and on momentum sum rules connecting the momentum distributions of gluons and quarks. See Ref. [20] (and references therein) for a recent review of the problem and of the solutions explored so far. This publication presents the EPS08 model, which uses inclusive hadron production data measured at forward rapidity by the BRAHMS experiment at RHIC to further constrain the nuclear effects on the gluon densities. Given that those measurements might reflect other physical processes (such as gluon saturation in a color-glass condensate), it is not at all clear that adding them in the derivation of the nuclear PDFs is justified. Therefore, in our study we prefer to place more emphasis
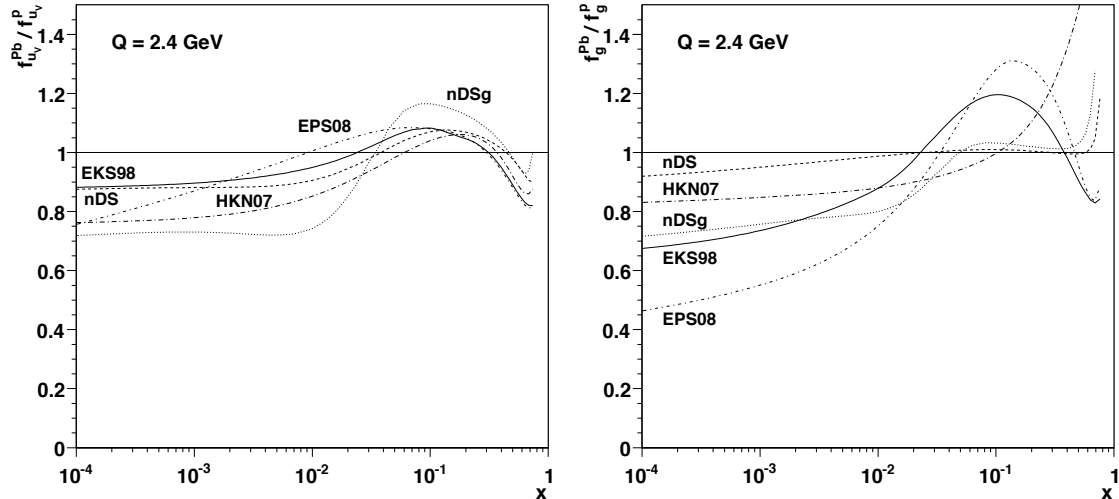
Figure 1: Ratio between the valence quark (left) and the gluon (right) distribution functions in a nucleon of a Pb nucleus and in a free proton, according to several models.

on the earlier EKS98 [21] parametrisation, the first global analysis of nuclear effects on the PDFs. The nDS/nDSg [22] and the HKN07 [23] parametrisations represent alternative analyses, also illustrated in Fig. 1, available both at leading order (used in our calculations) and at next-to-leading order.

Charmonium production at fixed-target energies probes x values in the "antishadowing" region, where the parton densities are enhanced in the heavy nucleus. Since $c\bar{c}$ production is dominated by gluon fusion, a good understanding of charmonium production in p-nucleus collisions is presently hampered by the lack of detailed knowledge of the nuclear gluon distributions, illustrated by the spread in the curves shown in the right panel of Fig. 1.

Figure 2 shows the influence on the J/ψ production cross section per nucleon (in the absence of any final state absorption) of using the EKS98 *nuclear* parton distribution functions rather than those of the free proton. The left panel shows that, at fixed-target energies, midrapidity charmonium production should be enhanced in p-Pb collisions with respect to the linear extrapolation of the pp yields (see Refs. [24, 25] for more details). The right panel shows that the "antishadowing" effect turns into a "shadowing" effect when charmonium production at forward x_F is considered.

3.3   Charmonium survival probabilities

In the framework of the Glauber model, described in detail in Ref. [26], the probability that a given charmonium state, generically represented by ψ, produced in a p-A collision, traverses the target nucleus unbroken by interactions with the nuclear
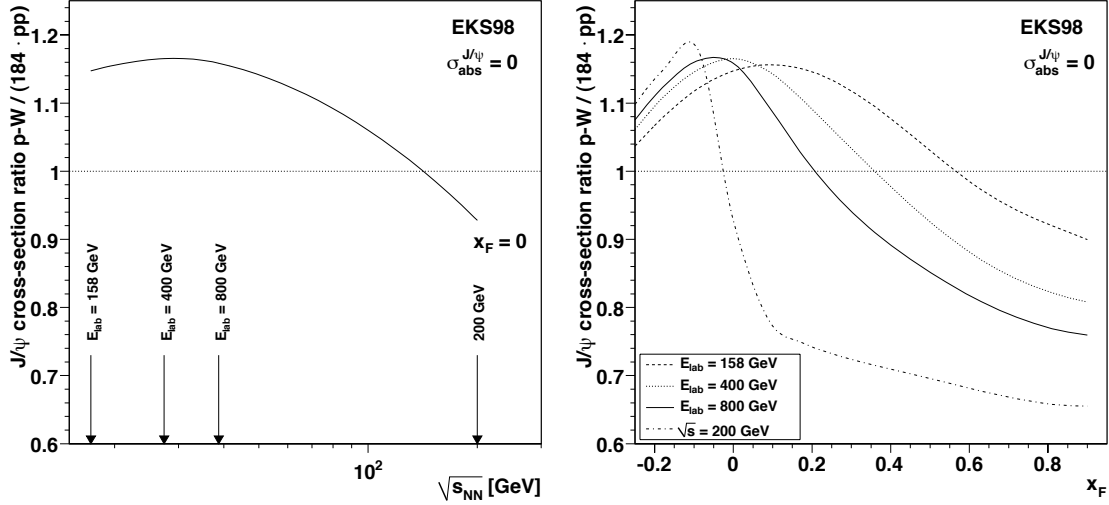
Figure 2: Changes induced by the nuclear modifications of the PDFs on the $c\bar{c}$ production cross section per nucleon in p-W collisions, using EKS98: as a function of $\sqrt{s_{NN}}$ at $x_F = 0$ (left) and as a function of x_F at four different energies (right).

matter, can be calculated as

$$S_{\text{abs}}^{\psi} = \frac{\sigma_{\text{pA}}^{\psi}}{A\,\sigma_{\text{pN}}^{\psi}} = \frac{1}{A} \int \mathrm{d}^2 b \int_{-\infty}^{\infty} \mathrm{d}z \; \rho_A(b,z)\; S_{\text{abs}}^{\psi}(b,z) \quad, \tag{5}$$

with

$$S_{\text{abs}}^{\psi}(b,z) = \exp\left\{-\int_z^{\infty} \mathrm{d}z'\; \rho_A(b,z')\;\sigma_{\text{abs}}^{\psi}\right\} \quad, \tag{6}$$

where b is the impact parameter of the collision (transverse distance between the flight path of the incident proton and the centre of the nucleus) and z is the $c\bar{c}$ production point along the beam axis. This "survival probability" depends essentially on the nuclear density profiles, ρ_A, and on the charmonium break-up cross section, $\sigma_{\text{abs}}^{\psi}$. In our calculations we used Woods-Saxon density profiles with the parameters given in Ref. [27]. No charmonium absorption has been considered in Hydrogen nuclei.

As we will see in detail later on, the absorption cross section crucially depends on whether the PDFs are taken to be those of a free nucleon or those of a nucleon in a nucleus. For instance, at SPS energies we obtain the same J/ψ nuclear absorption pattern using proton PDFs and $\sigma_{\text{abs}}^{J/\psi} = 4.5$ mb as we do using EKS98 nuclear PDFs and $\sigma_{\text{abs}}^{J/\psi} = 7$ mb, as shown in Fig. 3. If the *enhancement* of the per-nucleon charmonium production cross section caused by initial-state antishadowing is ignored, a weaker *final-state* "effective" absorption is sufficient to obtain the same result.
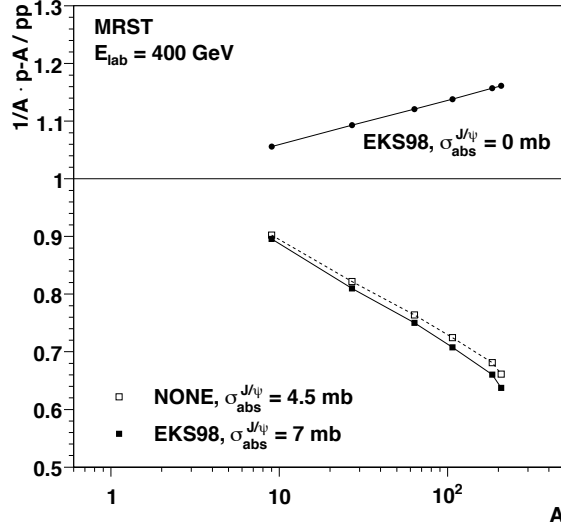
6

Figure 3: Illustration of the interplay between nuclear modifications of the parton densities and final-state charmonium absorption.

4   Measured charmonium production cross sections

Table 1 lists the experiments that measured the charmonium production cross sections, or ratios, used in our analysis. All experiments detected the J/ψ through its decay to dimuons or dielectrons, with good dilepton mass resolutions and small backgrounds.

Table 1: Basic features of the experiments providing the charmonium production cross sections (or ratios) considered in the present study.

Experiment	E_{lab} [GeV]	Collision systems	Phase space
NA3 [10]	200	p-H, Pt	$0.0 < x_F < 0.7$
NA50 [3]	400	p-Be, Al, Cu, Ag, W, Pb	$-0.425 < y_{cms} < 0.575$
NA50 [4]	450	p-Be, Al, Cu, Ag, W	$-0.50 < y_{cms} < 0.50$
E866 [9]	800	p-Be, W	$-0.10 < x_F < 0.93$
HERA-B [28]	920	p-C, W	$-0.34 < x_F < 0.14$

Experiment	$\sqrt{s_{NN}}$ [GeV]	Collision systems	Phase space
PHENIX [14]	200	pp, d-Au	$|y_{cms}| < 0.35,\ 1.2 < |y_{cms}| < 2.2$

Since our study focuses on the nuclear dependence of the quarkonium production cross section, it is preferable to have several target nuclei at each energy. NA50 collected data with five or six different target materials, from Be to Pb, providing a more detailed quarkonium absorption pattern as a function of the size of the target nucleus than the experiments which only used two targets. The J/ψ production cross sections measured by NA50 in p-nucleus collisions, at 400 and 450 GeV, in the centre-

Table 2: The J/ψ production cross sections, times branching ratio into dimuons, measured by NA50 at 400 and 450 GeV. The errors include statistical and target-to-target systematic uncertainties, added in quadrature.

	$B \times \sigma^{\mathrm{J}/\psi} / A$ [nb/nucleon]		
	NA50-400	NA50-450 "LI"	NA50-450 "HI"
Be	4.717 ± 0.10	5.27 ± 0.23	5.11 ± 0.18
Al	4.417 ± 0.10	5.14 ± 0.21	4.88 ± 0.23
Cu	4.280 ± 0.09	4.97 ± 0.22	4.74 ± 0.18
Ag	3.994 ± 0.09	4.52 ± 0.20	4.45 ± 0.15
W	3.791 ± 0.08	4.17 ± 0.37	4.05 ± 0.15
Pb	3.715 ± 0.08		

of-mass rapidity windows $-0.425 < y_{\mathrm{cms}} < 0.575$ and $|y_{\mathrm{cms}}| < 0.5$, respectively, are collected in Table 2. The 450 GeV values correspond to two statistically independent data sets, collected with "low" (LI) and "high" (HI) intensity proton beams. The 400 GeV errors are dominated by a target-dependent relative systematic uncertainty of 2.1 %. An extra global systematic uncertainty of 3 %, due to common normalisation uncertainties, is not included because it does not affect the evaluation of the nuclear dependence. This is because all the 400 GeV p-A data sets were collected in the same week, changing the target exposed to the beam roughly every hour, using a rotating target holder. On the contrary, the 450 GeV data sets were collected in different running periods, over five years, and have independent normalisation uncertainties (due to beam counting, trigger efficiencies, etc). Therefore, the quoted 450 GeV errors reflect the total uncertainties (added in quadrature).

The NA50 450 GeV cross sections were also reported in four equidistant x_{F} bins [4]. However, given their large uncertainties and small x_{F} coverage, they do not really provide extra information with respect to the integrated values, re-analysed in Ref. [3] to ensure consistency with the 400 GeV data analysis. Since NA50 reported absolute production cross sections (in nb) for each p-nucleus system, we extract the J/ψ nuclear absorption cross section, $\sigma_{\mathrm{abs}}^{\mathrm{J}/\psi}$, together with a σ_0 normalisation factor. In the case of the other experiments we used a one-parameter fit to extract $\sigma_{\mathrm{abs}}^{\mathrm{J}/\psi}$ from the *ratios* between the per-nucleon cross sections obtained with "heavy" and "light" nuclear targets. The HERA-B and E866 data samples cover a relatively large range in x_{F} and are very important for a differential study of the cold nuclear matter effects. Table 3 gives the E866 J/ψ W/Be ratios (see Ref. [9] for the $x_{\mathrm{F}} > 0.2$ values) and the HERA-B W/C ratios [28] (derived from the exponent α using Eq. 1) which we have used in our study. The errors represent statistical and point-to-point systematic uncertainties, added in quadrature. The global normalisation errors of 3 % (E866) and 4 % (HERA-B, obtained from a 1.5 % uncertainty on α) are not included in Table 3 but must be considered when comparing different experiments. E866 also measured Fe/Be ratios but only for $x_{\mathrm{F}} > 0.2$.

Table 3: J/ψ cross section ratios measured by E866 and HERA-B, without including global errors (3 % and 4 %, respectively).

	E866			HERA-B	
x_F range	$\langle x_\mathrm{F}\rangle$	W / Be ratio	x_F range	$\langle x_\mathrm{F}\rangle$	W / C ratio
-0.10 / -0.05	-0.0652	0.8929 ± 0.0184	-0.34 / -0.26	-0.285	1.105 ± 0.158
-0.05 / 0.00	-0.0188	0.8682 ± 0.0084	-0.26 / -0.22	-0.237	1.034 ± 0.096
0.00 / $+0.05$	$+0.0269$	0.8720 ± 0.0060	-0.22 / -0.18	-0.197	1.090 ± 0.063
$+0.05$ / $+0.10$	$+0.0747$	0.8739 ± 0.0057	-0.18 / -0.14	-0.158	1.043 ± 0.042
$+0.10$ / $+0.15$	$+0.1235$	0.8652 ± 0.0067	-0.14 / -0.10	-0.118	0.986 ± 0.030
$+0.15$ / $+0.20$	$+0.1729$	0.8725 ± 0.0100	-0.10 / -0.06	-0.079	0.943 ± 0.022
			-0.06 / -0.02	-0.040	0.915 ± 0.021
			-0.02 / $+0.02$	-0.002	0.916 ± 0.025
			$+0.02$ / $+0.06$	$+0.037$	0.902 ± 0.036
			$+0.06$ / $+0.14$	$+0.075$	0.866 ± 0.063

Table 4: J/ψ cross section ratios measured by NA3 and PHENIX, without including global errors (estimated to be 3 % and 11 %, respectively).

	NA3	PHENIX	
x_F range	H / Pt ratio	y_cms range	d-Au / pp ratio
0.0 / 0.1	1.27 ± 0.07	-2.2 / -1.7	0.95 ± 0.23
0.1 / 0.2	1.40 ± 0.06	-1.7 / -1.2	0.90 ± 0.21
0.2 / 0.3	1.34 ± 0.07	-0.35 / $+0.35$	0.85 ± 0.17
0.3 / 0.4	1.36 ± 0.12	$+1.2$ / $+1.7$	0.68 ± 0.13
0.4 / 0.5	1.75 ± 0.22	$+1.7$ / $+2.2$	0.59 ± 0.12
0.5 / 0.6	2.62 ± 0.52		
0.6 / 0.7	3.58 ± 1.81		

Table 4 gives the NA3 H/Pt ratios, for several x_F bins, as extracted "by eye" from Fig. 2 of Ref. [10]. A common systematic error of 3 % [29] is not included. NA3 used two targets: protons and platinum. When comparing the NA3 values to the other results, we should keep in mind that a proton is not exactly a "nucleus". We also analysed the presently available PHENIX d-Au/pp ratios in several rapidity bins [14], as collected in Table 4. These ratios have essentially no impact in the results of our study, given their large uncertainties.

It might be worth mentioning that we have not included in our study the measurements reported by the NA38 and E772 experiments. Later analyses of those data sets, made in the framework of the NA50 [7, 30] and E866 [9] experiments, respectively, revealed that those early results were biased, because of wrongly evaluated reconstruction efficiencies (NA38) or acceptances (E772).

5 Analysis of charmonium nuclear absorption

5.1 Cold nuclear matter effects

Now that we have reviewed the available J/ψ production measurements in proton-nucleus collisions, we can study them in view of deriving the so-called normal nuclear absorption, described in the framework of the Glauber formalism and quantified through the "J/ψ break-up cross section", $\sigma_{\text{abs}}^{J/\psi}$, introduced in Section 3.3. Before proceeding, however, we note that this is not the only mechanism affecting the per-nucleon production cross sections in p-nucleus collisions. As mentioned in Sections 3.1 and 3.2, the quarkonium production cross sections crucially depend on the parton densities (particularly the gluon densities), which are significantly affected by nuclear modifications. These modifications have been taken into account in our calculations, employing several parametrisations. Other nuclear effects, such as energy loss, formation times, etc., are likely to be present and would need to be considered in a detailed study of all aspects of quarkonium "cold nuclear effects". In particular, the nuclear charmonium production yields measured by E866 are clearly more suppressed at forward x_{F} than at $x_{\text{F}} = 0$, as observed in the W/Be and Fe/Be ratios shown in Fig. 4. There is a remarkable change in the suppression pattern at $x_{\text{F}} \approx 0.25$, from a relatively flat region around $x_{\text{F}} \approx 0$, where the ψ' is more absorbed than the J/ψ, to a forward region where both states show the same strong decrease with increasing x_{F}.
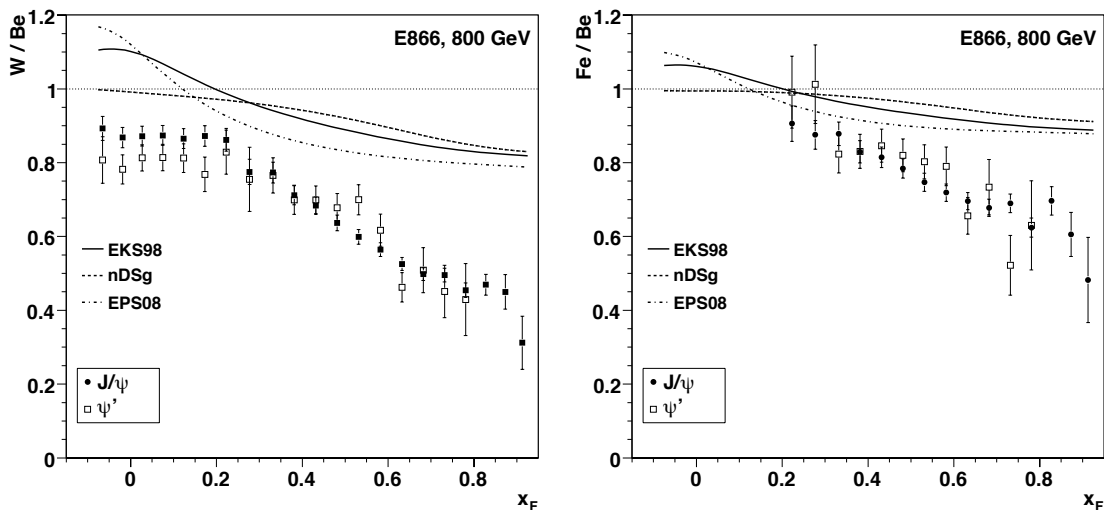

Figure 4: The x_{F} dependence of the J/ψ and ψ' production ratios, W/Be (left) and Fe/Be (right), per nucleon, measured by E866 at $E_{\text{lab}} = 800$ GeV (points) and calculated assuming only nuclear modifications of the parton densities (curves).

The curves in Fig. 4 show the expected trends when only considering the nuclear modifications on the parton distribution functions, without any final state absorption.

It is worth noting the antishadowing enhancement expected in the EKS98 and EPS08 models at $x_F \approx 0$.

In the present work, we concentrate on the "midrapidity region" and neglect nuclear effects other than initial-state modifications of the parton densities and final-state charmonium absorption, calculated as described in Sections 3.1 and 3.2. As in most previous studies of charmonium absorption in nuclear matter, we treat the J/ψ as a single meson passing through the nuclear medium. However, significant fractions of the J/ψ yield observed in elementary collisions are due to ψ' and χ_c decays, 8.1 ± 0.3 % and 25 ± 5 %, respectively, as recently determined from charmonium hadroproduction at $x_F \approx 0$ [31].

5.2 Extraction of $\sigma_{\mathrm{abs}}^{\mathbf{J}/\psi}$ from the measurements

From the equations in Section 3, we can see that the per-nucleon heavy-to-light target ratio of the charmonium production cross sections decreases as a function of the break-up cross section. This dependence has been calculated respecting the conditions of each measurement, considering the kinematics window, the collision energy and the nuclear matter densities. The calculations were performed using three sets of proton parton distribution functions: GRV LO 98 [32]; MRST2001 LO [18]; and CTEQ61L [19]. In addition to a control calculation with no nuclear modifications of the PDFs, labelled NONE, we employ four models of the nuclear modifications: EKS98 [21]; nDSg [22]; nDS [22]; and EPS08 [20].
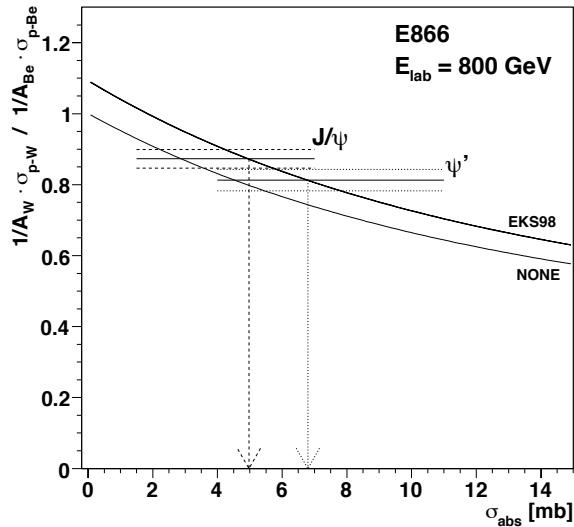

Figure 5: Illustration of extracting σ_{abs} for J/ψ and ψ' production from the E866 W/Be ratio with and without the EKS98 modifications of the PDFs.

The rather straightforward extraction of σ_{abs} for each measurement is illustrated in Fig. 5, using the E866 J/ψ and ψ' W/Be ratios in the range $-0.1 < x_F < 0.1$. The

PDFs effectively cancel in the calculations of the heavy/light ratios, even when nuclear effects are considered, since charmonium production is dominated by gg fusion. Given that the NA50 data were collected with five or six different targets, we performed a global two-parameter fit to all the p-A production cross sections within each data set (400, 450-LI and 450-HI).

Table 5: The J/ψ break-up cross sections, $\sigma_{\mathrm{abs}}^{\mathrm{J}/\psi}$, obtained in the Glauber framework described in Section 3. The NA50 400 and 450 GeV values correspond to the rapidity windows $-0.425 < y_{\mathrm{cms}} < 0.575$ and $|y_{\mathrm{cms}}| < 0.5$, respectively. Our study uses averages of the two 450 GeV sets.

Exp.	x_{F}	$\sigma_{\mathrm{abs}}^{\mathrm{J}/\psi}$ [mb]				
		NONE	nDS	nDSg	EKS98	EPS08
NA3	0.05	3.77 ± 0.98	3.94 ± 0.99	4.27 ± 1.00	5.79 ± 1.07	7.00 ± 1.12
	0.15	5.35 ± 0.88	5.46 ± 0.88	5.85 ± 0.89	7.38 ± 0.95	8.15 ± 0.98
	0.25	4.66 ± 0.98	4.63 ± 0.98	5.01 ± 0.99	6.18 ± 1.04	6.38 ± 1.05
	0.35	$4.96^{+1.51}_{-1.56}$	$4.71^{+1.49}_{-1.54}$	$5.07^{+1.51}_{-1.56}$	$5.81^{+1.56}_{-1.61}$	$5.62^{+1.55}_{-1.60}$
NA50-400		4.83 ± 0.63	4.74 ± 0.62	4.73 ± 0.62	7.01 ± 0.70	7.98 ± 0.74
450-LI		4.51 ± 1.58	4.39 ± 1.58	4.39 ± 1.58	6.89 ± 1.76	7.93 ± 1.83
450-HI		4.82 ± 1.10	4.71 ± 1.09	4.71 ± 1.09	7.17 ± 1.22	8.21 ± 1.28
E866	-0.0652	$2.37^{+0.83}_{-0.77}$	$2.32^{+0.83}_{-0.77}$	$3.01^{+0.85}_{-0.79}$	$4.67^{+0.92}_{-0.85}$	$6.06^{+0.98}_{-0.90}$
	-0.0188	$3.00^{+0.73}_{-0.69}$	$2.85^{+0.73}_{-0.69}$	$3.62^{+0.75}_{-0.71}$	$5.39^{+0.82}_{-0.76}$	$6.20^{+0.85}_{-0.79}$
	$+0.0269$	$2.90^{+0.71}_{-0.67}$	$2.65^{+0.70}_{-0.66}$	$3.27^{+0.72}_{-0.68}$	$4.98^{+0.78}_{-0.73}$	$5.03^{+0.78}_{-0.73}$
	$+0.0747$	$2.85^{+0.71}_{-0.67}$	$2.50^{+0.70}_{-0.66}$	$2.65^{+0.70}_{-0.66}$	$4.36^{+0.76}_{-0.71}$	$3.81^{+0.74}_{-0.70}$
	$+0.1235$	$3.07^{+0.72}_{-0.68}$	$2.61^{+0.71}_{-0.67}$	$2.13^{+0.69}_{-0.65}$	$3.95^{+0.75}_{-0.71}$	$2.98^{+0.72}_{-0.68}$
	$+0.1729$	$2.89^{+0.74}_{-0.70}$	$2.31^{+0.73}_{-0.68}$	$1.28^{+0.69}_{-0.65}$	$3.13^{+0.75}_{-0.71}$	$1.91^{+0.71}_{-0.67}$
HERA-B	-0.158	—	—	—	$0.73^{+1.42}_{-0.73}$	$2.23^{+1.52}_{-1.35}$
	-0.118	$0.34^{+1.22}_{-0.34}$	$0.42^{+1.22}_{-0.42}$	$0.96^{+1.25}_{-0.96}$	$2.34^{+1.33}_{-1.20}$	$3.88^{+1.43}_{-1.28}$
	-0.079	$1.39^{+1.18}_{-1.08}$	$1.38^{+1.18}_{-1.08}$	$2.04^{+1.22}_{-1.11}$	$3.68^{+1.32}_{-1.19}$	$5.08^{+1.41}_{-1.26}$
	-0.040	$2.11^{+1.21}_{-1.10}$	$1.99^{+1.20}_{-1.09}$	$2.76^{+1.24}_{-1.13}$	$4.53^{+1.36}_{-1.22}$	$5.46^{+1.42}_{-1.27}$
	-0.002	$2.10^{+1.28}_{-1.15}$	$1.85^{+1.26}_{-1.14}$	$2.58^{+1.31}_{-1.18}$	$4.32^{+1.42}_{-1.27}$	$4.58^{+1.44}_{-1.29}$
	$+0.037$	$2.46^{+1.51}_{-1.34}$	$2.09^{+1.49}_{-1.32}$	$2.51^{+1.52}_{-1.35}$	$4.28^{+1.65}_{-1.45}$	$3.94^{+1.63}_{-1.43}$
	$+0.075$	$3.52^{+2.43}_{-2.02}$	$2.96^{+2.36}_{-1.97}$	$2.52^{+2.31}_{-1.93}$	$4.58^{+2.56}_{-2.11}$	$3.59^{+2.44}_{-2.02}$

Table 5 collects the $\sigma_{\mathrm{abs}}^{\mathrm{J}/\psi}$ values obtained with the CTEQ61L PDFs, including the aforementioned nuclear modifications. Other PDFs give essentially the same results. The global uncertainties on the cross-section ratios were propagated into the errors on $\sigma_{\mathrm{abs}}^{\mathrm{J}/\psi}$ using a Monte Carlo procedure; they are common to all the x_{F} bins at the level of the ratios but not at the level of $\sigma_{\mathrm{abs}}^{\mathrm{J}/\psi}$. This way, we can directly compare results obtained by different experiments. We can clearly see a correlation between the extracted $\sigma_{\mathrm{abs}}^{\mathrm{J}/\psi}$ values and the assumed initial-state nuclear effects on the PDFs

(already indicated in Fig. 3): a strong antishadowing effect leads to a large $\sigma_{\mathrm{abs}}^{\mathrm{J}/\psi}$. The most backward HERA-B bins, $x_{\mathrm{F}} < -0.14$, where $\alpha > 1$, do not require any final-state absorption unless strong antishadowing effects, such as those in EKS98 and EPS08, enhance the initial-state production rates in heavy targets. Given the large uncertainties of the presently available PHENIX ratios, we do not include the corresponding $\sigma_{\mathrm{abs}}^{\mathrm{J}/\psi}$ values in Table 5.

5.3 Dependence of $\sigma_{\mathrm{abs}}^{\mathrm{J}/\psi}$ on kinematics

The ratio between the p-W and the p-Be J/ψ (and ψ') cross sections measured by E866, shown in Fig. 4, indicates the existence of additional charmonium absorption mechanisms at forward x_{F}, perhaps related to formation time and energy loss effects. On the other hand, the measured pattern is remarkably flat in the region $x_{\mathrm{F}} < 0.25$, an observation naturally interpreted as meaning that the processes responsible for the strong absorption at forward x_{F} are negligible at midrapidity. This justifies confining our present studies to the "midrapidity region", where the nuclear effects are seemingly simpler and "Glauber final-state charmonium absorption", as described in Section 3.3, may be sufficient to describe most measurements. Furthermore, the SPS heavy-ion data samples have been collected close to midrapidity. Obviously, the flat W/Be ratios at "midrapidity" directly translate into an equally flat $\alpha(x_{\mathrm{F}})$, as shown in the left panel of Fig. 6.
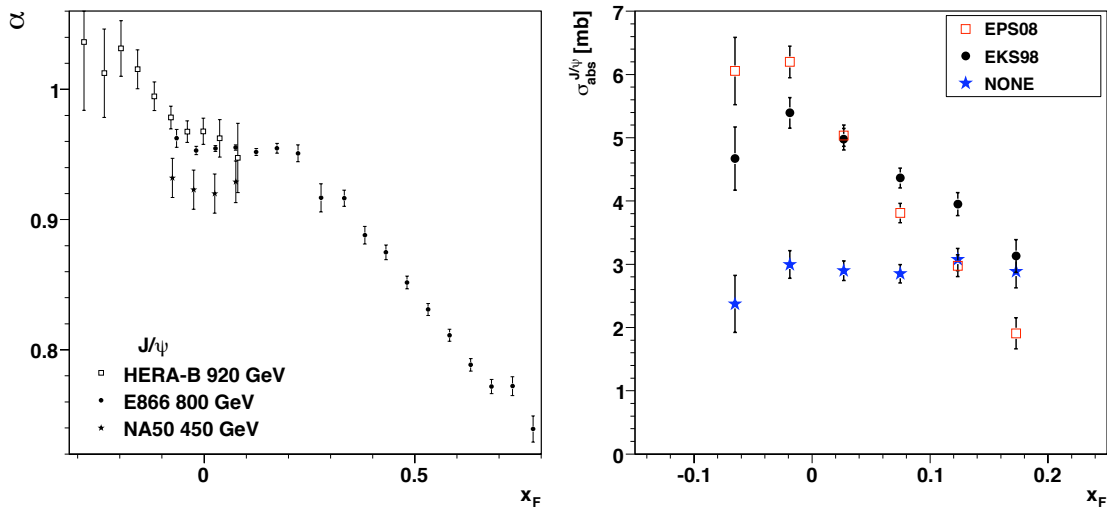

Figure 6: The nuclear dependence of the charmonium production cross sections measured by E866, expressed in terms of α (left) and $\sigma_{\mathrm{abs}}^{\mathrm{J}/\psi}$ (right), without the 3 % global uncertainty. The left panel also includes the NA50 and HERA-B patterns.

Our calculations also give rather constant $\sigma_{\mathrm{abs}}^{\mathrm{J}/\psi}$ values in the range $-0.1 < x_{\mathrm{F}} < +0.2$, with $\sigma_{\mathrm{abs}}^{\mathrm{J}/\psi} \sim 3$ mb, when we neglect nuclear modifications of the PDFs, as shown numerically in Table 5 and graphically in the right panel of Fig. 6. However, when

we use nuclear parton distributions with strong antishadowing, we see that $\sigma^{J/\psi}_{abs}$ is significantly larger at $x_F = -0.1$ than at $+0.2$, (see Fig. 6-right). Another observation can be made from the x_F dependence of the E866 data. If we assume that nuclear absorption effects on the J/ψ can be effectively described by the Glauber formalism with a single $\sigma^{J/\psi}_{abs}$ (ignoring formation times, feed-down contributions, energy loss, etc), we see a rather striking *increase* of $\sigma^{J/\psi}_{abs}$ at forward x_F, explicitly shown in Fig. 7 but already clear in Fig. 4 from the difference between the calculations and the data. The observation of a stronger absorption at forward rapidity (or x_F) does not depend on the nuclear modifications model used.

The HERA-B measurements also span a relatively large x_F range, covering a more backward window but having a sizable overlap with E866 around $x_F \approx 0$. Figure 7 shows the E866 and HERA-B $\sigma^{J/\psi}_{abs}$ values, obtained using the EKS98 nuclear PDFs, as a function of x_F and laboratory rapidity, y_{lab}, calculated from x_F accounting for the J/ψ $\langle p_T^2 \rangle$ (which increases with $\sqrt{s_{NN}}$). The "midrapidity" ($x_F < 0.25$ or $y_{lab} < 5$) E866 and HERA-B patterns can be empirically parametrised by the same asymmetric Gaussian shape but independent magnitudes.
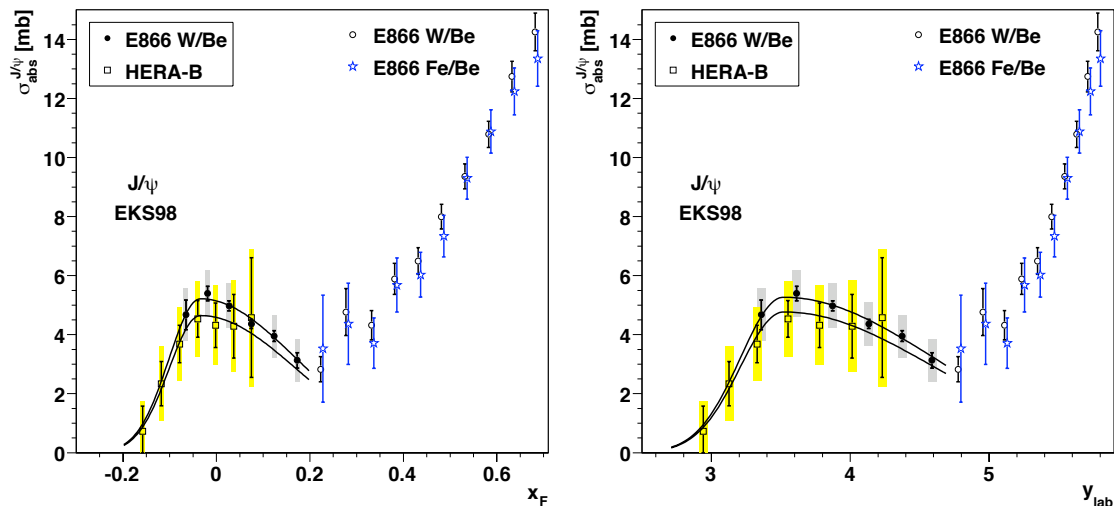

Figure 7: The extracted $\sigma^{J/\psi}_{abs}$ as a function of x_F (left) and y_{lab} (right), as derived from the E866 and HERA-B data. The forward E866 data points (open circles and stars) are not included in the fitted curves. The boxes represent the total errors.

Before continuing, we reiterate our original goal in light of what we have observed so far. We seek to determine and quantify possible changes of the "midrapidity J/ψ break-up cross section" as a function of collision energy. More specifically, we want to find out whether it is justified to analyse heavy-ion measurements at 158 GeV using the $\sigma^{J/\psi}_{abs}$ values derived from proton-nucleus data collected at much higher energies (400 and 450 GeV). We have now seen that, in reality, there is no single "midrapidity" $\sigma^{J/\psi}_{abs}$ value, unless we neglect nuclear effects on the PDFs. In particular, the E866 data

indicate that, for nDSg, EKS98 or EPS08, $\sigma_{\mathrm{abs}}^{J/\psi}$ drops by a factor of 2 or 3 in the range $0 < x_{\mathrm{F}} < 0.25$, corresponding to the centre-of-mass rapidity range $0 < y_{\mathrm{cms}} < 1$. Such a non-negligible change in $\sigma_{\mathrm{abs}}^{J/\psi}$ with the longitudinal momentum of the J/ψ indicates that our quest is not an easy one. There are several possible scenarios worth considering. For example, it could turn out that all data sets, regardless of collision energy, exhibit the same $\sigma_{\mathrm{abs}}^{J/\psi}$ dependence on y_{cms}, in shape and magnitude. If so, we can determine the $\sigma_{\mathrm{abs}}^{J/\psi}$ suitable for the analysis of the heavy-ion data by integrating that universal function in the range $0 < y_{\mathrm{cms}} < 1$, the NA50 spectrometer window at 158 GeV. This is likely to result in a different $\sigma_{\mathrm{abs}}^{J/\psi}$ than that obtained by integrating the same function in the 450 GeV window, $|y_{\mathrm{cms}}| < 0.5$. On the other hand, if the magnitude of $\sigma_{\mathrm{abs}}^{J/\psi}$ is energy dependent, the change in the rapidity window could, perhaps, partially compensate the change in energy, leading to similar $\sigma_{\mathrm{abs}}^{J/\psi}$ values at 158 GeV in $0 < y_{\mathrm{cms}} < 1$ and at 450 GeV in $|y_{\mathrm{cms}}| < 0.5$. It is also possible that the *shape* of $\sigma_{\mathrm{abs}}^{J/\psi}(y_{\mathrm{cms}})$ depends on energy, in which case y_{cms} is not a suitable variable to describe charmonium absorption.

5.4 Dependence of $\sigma_{\mathrm{abs}}^{J/\psi}$ on the collision energy

To evaluate which scenario best describes the measurements requires a global survey of all available p-A results, obtained at different energies and in different x_{F} or rapidity ranges.

The $\sigma_{\mathrm{abs}}^{J/\psi}$ values collected in Table 5 are shown in Fig. 8 as a function of the y_{cms} variable, for four different parametrisations of the nuclear effects on the PDFs. The E866, HERA-B and NA3 values derived using free proton PDFs (top-left panel) can be considered flat in the midrapidity range $-0.3 < y_{\mathrm{cms}} < 1.0$. Therefore, in this case (as for nDS) we can evaluate $\sigma_{\mathrm{abs}}^{J/\psi}(y_{\mathrm{cms}}{=}0)$ by simply fitting each data set to a constant.

The nuclear modifications of the PDFs considerably affect the $\sigma_{\mathrm{abs}}^{J/\psi}(y_{\mathrm{cms}})$ pattern and a non-trivial y_{cms} dependence is needed to evaluate the $\sigma_{\mathrm{abs}}^{J/\psi}(y_{\mathrm{cms}}{=}0)$ values for the various data sets. Using EKS98 PDFs, for example, the E866 and HERA-B data sets suggest the use of an asymmetric Gaussian function with $\mu \approx -0.21$ mb, $\sigma_{L} \approx 0.37$ mb and $\sigma_{R} \approx 1.1$ mb. Since the NA50 $\sigma_{\mathrm{abs}}^{J/\psi}$ values correspond to broad rapidity ranges, the asymmetric Gaussian shape is weighted by the rapidity distribution of the *measured* J/ψ dimuons (those which contributed to the derived σ_{abs} value), provided in Ref. [7]. However, this convolution has almost no impact on the final result.

The change in the magnitude of $\sigma_{\mathrm{abs}}^{J/\psi}(y_{\mathrm{cms}}{=}0)$ with collision energy, $\sqrt{s_{NN}}$, can be observed in Fig. 9, for free proton PDFs ("NONE") and for the nDSg, EKS98 and EPS08 parametrisations of the nuclear PDFs. The corresponding numerical values are collected in Table 6. To determine the $\sigma_{\mathrm{abs}}^{J/\psi}$ relevant for the analysis of the SPS heavy-ion results, we extrapolate $\sigma_{\mathrm{abs}}^{J/\psi}(y_{\mathrm{cms}}{=}0)$ down to $\sqrt{s_{NN}} = 17.2$ GeV (dotted vertical line in Fig. 9), using exponential and linear functions.

The dependence of $\sigma_{\mathrm{abs}}^{J/\psi}$ on y_{cms} at $\sqrt{s_{NN}} = 17.2$ GeV is shown in Fig. 10, for several
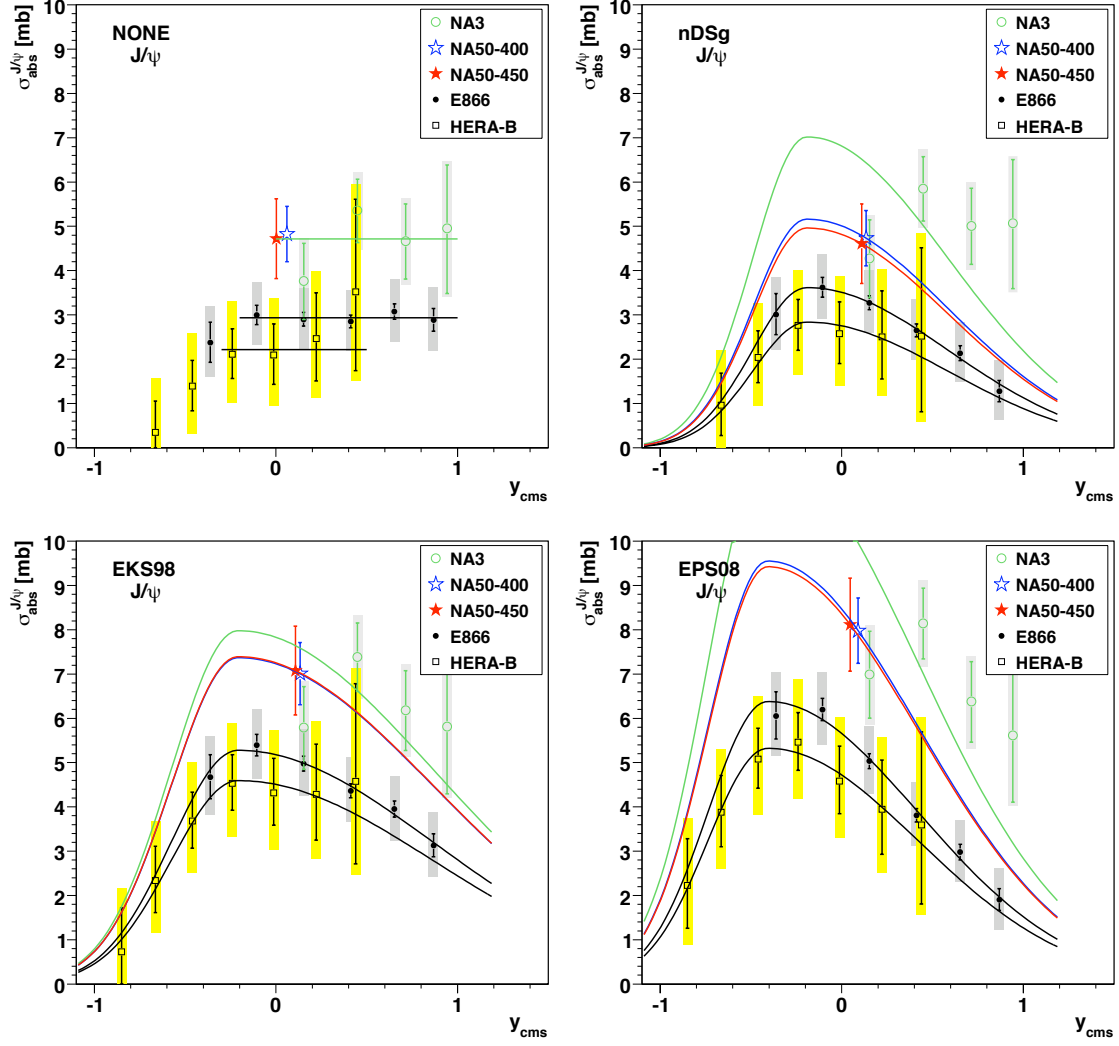
Figure 8: $\sigma_{\text{abs}}^{J/\psi}$ as a function of y_{cms}, obtained by considering four alternative parametrisations of the nuclear PDFs. The boxes represent the total errors. When nuclear PDFs are used, the E866 and HERA-B absorption patterns clearly depend on y_{cms}.

nuclear PDFs, while the values of $\sigma_{\text{abs}}^{J/\psi}(y_{\text{cms}}=0)$ are collected in Table 7. Integrating these functions in the NA50 heavy-ion rapidity window at 158 GeV, $0 < y_{\text{cms}} < 1$, weighted by the rapidity distribution of the J/ψ dimuons measured in Pb-Pb collisions (before acceptance corrections) [33], we obtain the values of $\sigma_{\text{abs}}^{J/\psi}(0 < y_{\text{cms}} < 1)$ given in Table 7.
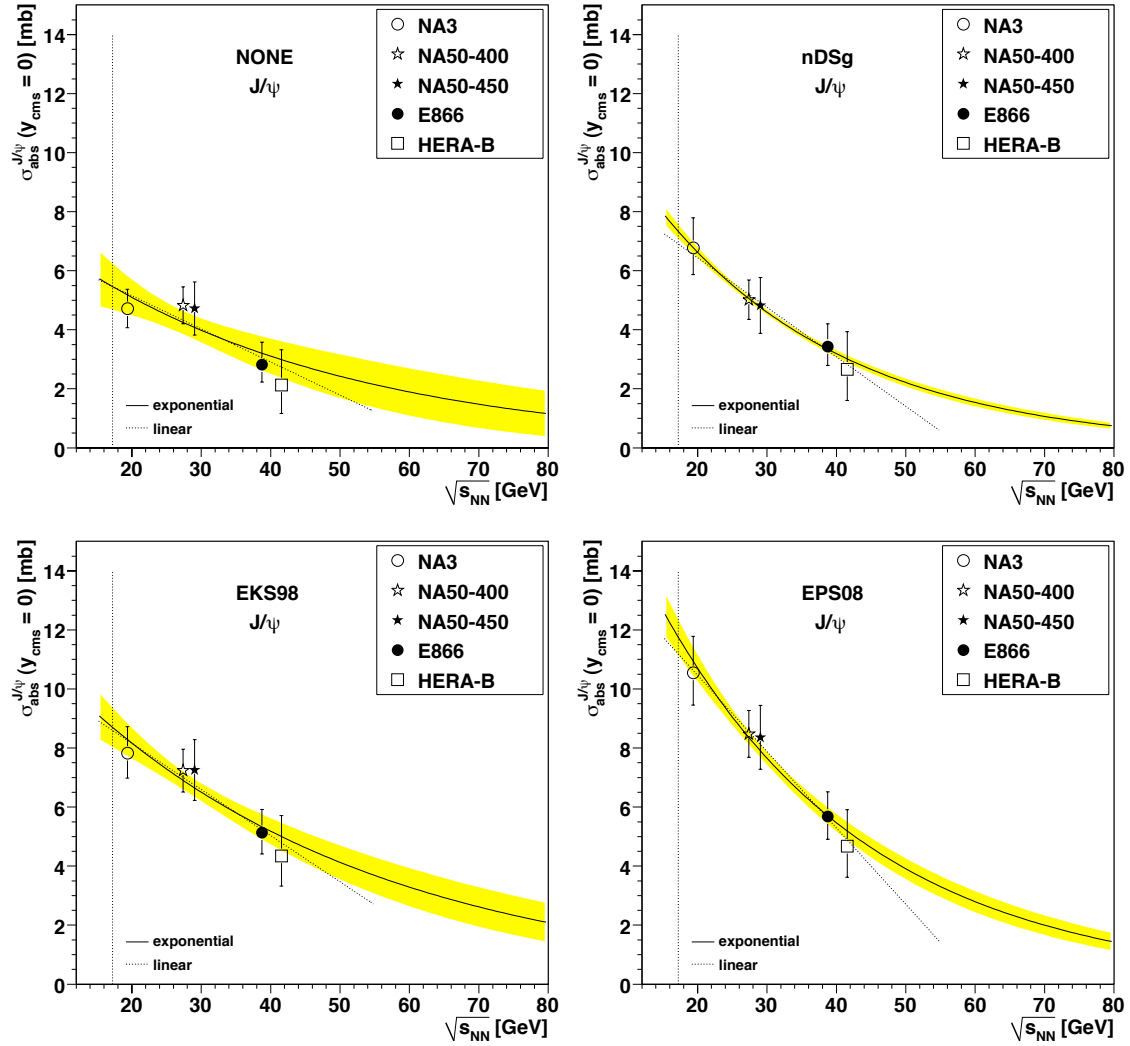
16

Figure 9: Dependence of $\sigma_{\text{abs}}^{\text{J}/\psi}(y_{\text{cms}}=0)$ on the nucleon-nucleon centre-of-mass energy. The curves represent fits with exponential (solid line with error band) and linear (dotted line) functions.

Table 6: $\sigma_{\text{abs}}^{\text{J}/\psi}(y_{\text{cms}}=0)$ values extracted from the five analysed data sets and for the nuclear PDFs we have considered, including the free protons case.

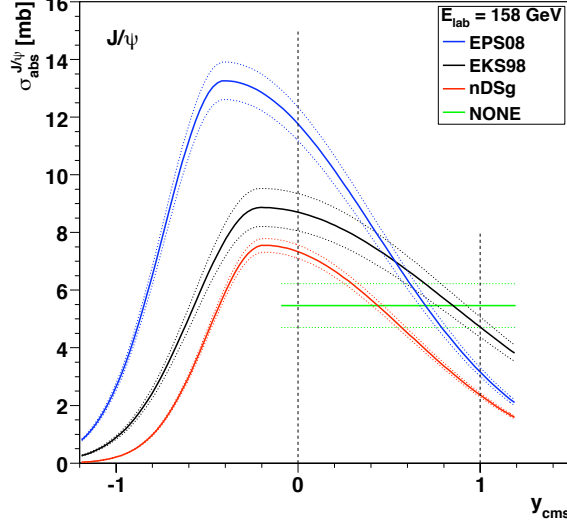| Exp.	$\sigma_{\text{abs}}^{\text{J}/\psi}(y_{\text{cms}}=0)$ [mb]				
	NONE	nDS	nDSg	EKS98	EPS08
NA3	4.71 ± 0.66	4.76 ± 0.66	$6.78^{+1.01}_{-0.91}$	$7.82^{+0.90}_{-0.84}$	$10.55^{+1.24}_{-1.10}$
NA50-400	4.82 ± 0.63	4.74 ± 0.62	5.02 ± 0.67	7.24 ± 0.73	8.48 ± 0.79
NA50-450	4.72 ± 0.90	4.61 ± 0.90	4.82 ± 0.95	7.25 ± 1.03	8.36 ± 1.08
E866	$2.82^{+0.76}_{-0.59}$	$2.53^{+0.75}_{-0.63}$	$3.43^{+0.77}_{-0.64}$	$5.13^{+0.79}_{-0.72}$	$5.68^{+0.84}_{-0.77}$
HERA-B	$2.13^{+1.19}_{-0.96}$	$1.93^{+1.15}_{-0.97}$	$2.66^{+1.28}_{-1.05}$	$4.35^{+1.37}_{-1.03}$	$4.67^{+1.24}_{-1.05}$

17

Figure 10: $\sigma_{\mathrm{abs}}^{\mathrm{J}/\psi}$ as a function of y_{cms}, extrapolated to 158 GeV considering four alternative parametrisations of the nuclear PDFs.

Table 7: The $\sigma_{\mathrm{abs}}^{\mathrm{J}/\psi}(y_{\mathrm{cms}}{=}0)$ and $\sigma_{\mathrm{abs}}^{\mathrm{J}/\psi}(0 < y_{\mathrm{cms}} < 1)$ values evaluated at 158 GeV by extrapolating with an exponential function the values derived from measurements made at higher energies, by NA3, NA50, E866 and HERA-B.

N-PDFs	$\sigma_{\mathrm{abs}}^{\mathrm{J}/\psi}(y_{\mathrm{cms}}{=}0)$ [mb]	$\sigma_{\mathrm{abs}}^{\mathrm{J}/\psi}(0 < y_{\mathrm{cms}} < 1)$ [mb]
NONE	5.5 ± 0.8	5.5 ± 0.8
nDS	5.6 ± 0.8	5.6 ± 0.8
nDSg	7.3 ± 0.2	5.2 ± 0.2
EKS98	8.7 ± 0.7	7.2 ± 0.5
EPS08	11.8 ± 0.6	7.5 ± 0.4

5.5 Dependence of $\sigma_{\mathrm{abs}}^{\mathbf{J}/\psi}$ on the $\mathbf{J}/\psi$ energy

We now consider a different scenario. If we assume that the J/ψ is "broken up" by interactions with nucleons while traversing the nuclear target, it is natural to study the absorption as a function of the J/ψ-nucleon centre-of-mass energy, $\sqrt{s_{\psi N}}$, a quantity that reflects both the nucleon-nucleon centre-of-mass energy, $\sqrt{s_{NN}}$, and the energy of the J/ψ. This energy may be written as a function of the J/ψ x_{F} as

$$\sqrt{s_{\psi N}} = \sqrt{m_\psi^2 + \sqrt{s_{NN}} \left(x_{\mathrm{F}} \sqrt{\frac{s_{NN}}{4} - m_\psi^2} + \sqrt{p_{\mathrm{T}}^2 + x_{\mathrm{F}}^2 \left(\frac{s_{NN}}{4} - m_\psi^2\right) + m_\psi^2} \right)} \quad , \quad (7)$$

18

where m_ψ and p_T are the mass and transverse momentum of the J/ψ. When $x_F = 0$ and the p_T dependence is neglected, this expression reduces to

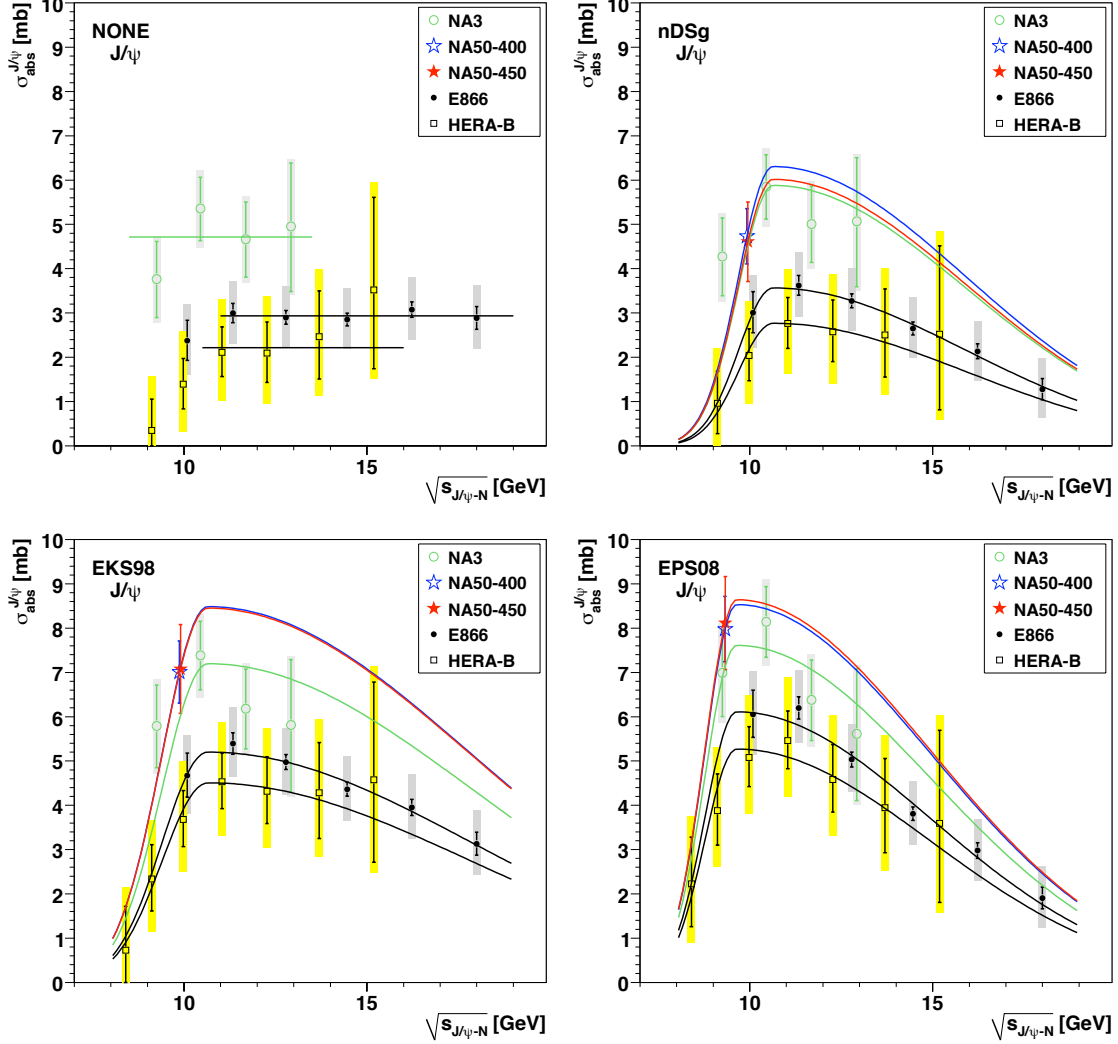$$\sqrt{s_{\psi N}} = m_\psi \sqrt{1 + \frac{\sqrt{s_{NN}}}{m_\psi}} \quad . \tag{8}$$

Figure 11: $\sigma_{\mathrm{abs}}^{\mathrm{J}/\psi}$ as a function of the J/ψ-nucleon centre-of-mass energy, determined from the fixed-target data sets, with four different nuclear PDFs. The boxes represent the total errors.

Figure 11 shows $\sigma_{\mathrm{abs}}^{\mathrm{J}/\psi}$ as a function of $\sqrt{s_{\psi N}}$ for the fixed-target data sets. The centres and widths of the asymmetric Gaussians are exclusively determined by the E866 and HERA-B points while the magnitudes are independently fitted for each data set. The NA3 values are closer to the others here than as a function of y_{cms}

(Fig. 8). However, it is clear that there is also no scaling as a function of $\sqrt{s_{\psi N}}$ since the different data sets result in significantly different magnitudes of $\sigma_{\text{abs}}^{\text{J}/\psi}$; the E866 and HERA-B values are too low while NA50 is too high relative to a global average. The decrease of $\sigma_{\text{abs}}^{\text{J}/\psi}$ with increasing beam energy is always seen, regardless of the nuclear PDF set, including that of the free proton (NONE).

The absence of a universal curve indicates that the mechanisms determining the J/ψ nuclear dependence are not accurately described by the simple "Glauber absorption model" we used in our analysis. An improved model is needed to properly explain charmonium absorption and its dependencies on collision energy and kinematics, including the extra absorption seen at forward x_{F}.

6   Summary and outlook

Previous derivations of the J/ψ normal nuclear absorption baseline used to search for QGP signals in the SPS heavy-ion measurements, collected at $E_{\text{lab}} = 158$ GeV, were based on proton-nucleus data collected at 400–450 GeV, assuming that $\sigma_{\text{abs}}^{\text{J}/\psi}$ is a "universal quantity", insensitive to changes related to the collision energy or to the rapidity window. This paper presents an improved analysis of charmonium production in proton-nucleus collisions. First, we studied J/ψ proton-nucleus data collected in several fixed-target experiments, covering a broad range of collision energies ($\sqrt{s_{NN}} = 20$–40 GeV), as well as d-Au data collected by PHENIX at $\sqrt{s_{NN}} = 200$ GeV (presently affected by large uncertainties). Second, we considered nuclear modifications of the PDFs, employing several models which consistently indicate initial-state gluon enhancement (antishadowing) in the midrapidity region of the fixed-target data.

We observe that, when the nuclear modifications of the PDFs are taken into account, $\sigma_{\text{abs}}^{\text{J}/\psi}$ significantly depends on the rapidity of the J/ψ, even within a relatively narrow midrapidity window. In particular, the J/ψ nuclear dependence determined by E866 in the window $-0.1 < x_{\text{F}} < +0.2$ only looks independent of x_{F} if the nuclear effects on the PDFs are neglected. Furthermore, the level of cold nuclear matter absorption of midrapidity J/ψ significantly decreases with collision energy. While the specific numerical values depend on the nuclear PDF sets used, the decrease of $\sigma_{\text{abs}}^{\text{J}/\psi}$ with energy is a general feature, independent of any nuclear modifications of the PDFs. The observation that $\sigma_{\text{abs}}^{\text{J}/\psi}$ depends on the rapidity of the J/ψ and on the collision energy confirms that the simple Glauber-type absorption model commonly used in J/ψ suppression studies is insufficient to properly reproduce the available measurements. The sought-for "universal quantity" is, after all, a multidimensional function without obvious scaling features.

For the moment, in the absence of a more detailed formalism, we used the data-driven $\sigma_{\text{abs}}^{\text{J}/\psi}(y_{\text{cms}})$ dependence and a simple extrapolation of the $\sqrt{s_{NN}}$ dependence to evaluate the $\sigma_{\text{abs}}^{\text{J}/\psi}$ value corresponding to the rapidity window covered by NA50 at 158 GeV, obtaining the values summarised in Table 7. The $\sigma_{\text{abs}}^{\text{J}/\psi}$ values obtained in this study should be seen as effective ones, incorporating the nuclear matter effects

on the directly produced J/ψ as well as on the more massive χ_c and ψ' states. Indeed, around 33 % of the observed J/ψ yields result from decays of χ_c and ψ' states [31], which are expected to suffer stronger nuclear absorption than the directly produced J/ψ.

Having relaxed the assumption of a universal absorption cross section, we can test whether it is justified to study the SPS heavy-ion data, collected at 158 GeV, using the $\sigma_{\mathrm{abs}}^{\mathrm{J}/\psi}$ value obtained from the higher-energy NA50 measurements. As shown in Table 7, if we neglect nuclear modifications on the PDFs we derive $\sigma_{\mathrm{abs}}^{\mathrm{J}/\psi}(0 < y_{\mathrm{cms}} < 1) = 5.5 \pm 0.8$ mb, higher than the value used so far in the analyses of the SPS heavy-ion measurements (4.2 ± 0.5 mb, also using free proton PDFs). If we use the EKS98 parametrisation to model the nuclear modifications of the PDFs, we obtain $\sigma_{\mathrm{abs}}^{\mathrm{J}/\psi}(0 < y_{\mathrm{cms}} < 1) = 7.2 \pm 0.5$ mb. It is interesting to notice that this is identical to the value obtained by NA50 at 400 GeV in the rapidity window $-0.425 < y_{\mathrm{cms}} < 0.575$ (7.01 ± 0.70 mb, see Table 5). The drop of $\sigma_{\mathrm{abs}}^{\mathrm{J}/\psi}$ from $y_{\mathrm{cms}} = 0$ to $y_{\mathrm{cms}} = 1$, in the EKS98 case, exactly compensates the increase in $\sigma_{\mathrm{abs}}^{\mathrm{J}/\psi}$ from $E_{\mathrm{lab}} = 400$ to 158 GeV. Nevertheless, a quantitative re-evaluation of the level of "QGP melting" in the heavy-ion data should be performed, also considering nuclear modifications of the PDFs in the beam nucleus (in an x range different from that of the target nucleus).

Our understanding of the cold nuclear effects on J/ψ production, and their energy dependence, should significantly improve in the near future, thanks to new NA60 results based on proton-nucleus data collected at 158 GeV and to new PHENIX results based on a large d-Au data set.

Acknowledgements

References

[1] F. Karsch, *Lattice QCD at high temperature and density*, Lecture Notes in Physics **583** (2002) 209, Springer Germany.

[2] T. Matsui and H. Satz, *J/ψ Suppression by Quark-Gluon Plasma Formation*, *Phys. Lett.* **B 178** (1986) 416.

[3] B. Alessandro *et al.* (NA50 Coll.), *J/ψ and ψ′ production and their normal nuclear absorption in proton-nucleus collisions at 400 GeV*, *Eur. Phys. J.* **C 48** (2006) 329.

[4] B. Alessandro *et al.* (NA50 Coll.), *Charmonium production and nuclear absorption in p-A interactions at 450 GeV*, *Eur. Phys. J.* **C 33** (2004) 31.

[5] B. Alessandro *et al.* (NA50 Coll.), *A new measurement of J/ψ suppression in Pb-Pb collisions at 158 GeV per nucleon*, *Eur. Phys. J.* **C 39** (2005) 335.

[6] R. Arnaldi *et al.* (NA60 Coll.), *J/ψ production in Indium-Indium collisions at 158 GeV/nucleon*, *Phys. Rev. Lett.* **99** (2007) 132302.

[7] G. Borges, PhD thesis, *J/ψ and ψ′ Production in p-A Collisions at 400 GeV and S-U interactions at 200 GeV/nucleon*, Universidade Técnica de Lisboa, 2005, `http://cern.ch/NA50/theses.html`

[8] B. Alessandro *et al.* (NA50 Coll.), *ψ′ production in Pb-Pb collisions at 158 GeV/nucleon*, *Eur. Phys. J.* **C 49** (2007) 559.

[9] M.J. Leitch *et al.* (E866 Coll.), *Measurement of J/ψ and ψ′ suppression in p-A collisions at 800 GeV/c*, *Phys. Rev. Lett.* **84** (2000) 3256 and http://p25ext.lanl.gov/e866/papers/e866prlj/ratiosc.txt

[10] J. Badier *et al.* (NA3 Coll.), *Experimental J/ψ Hadronic Production from 150 GeV/c to 280 GeV/c*, *Z. Physik* **C 20** (1983) 101.

[11] R. Shahoyan, PhD thesis, *J/ψ and ψ′ production in 450 GeV p-A interactions and its dependence on rapidity and x_{F}*, Universidade Técnica de Lisboa, 2001, `http://cern.ch/NA50/theses.html`

[12] F. Arleo and V.N. Tram, *A Systematic study of J/psi suppression in cold nuclear matter*, *Eur. Phys. J.* **C 55** (2008) 449.

[13] C. Lourenço *et al.* (NA60 Coll.), *Request for 7 days of primary protons at 158 GeV*, CERN-SPSC-2004-012, SPSC-M-715, 2004.

[14] A. Adare *et al.* (PHENIX Coll.), *Cold Nuclear Matter Effects on J/ψ as Constrained by Deuteron-Gold Measurements at $\sqrt{s_{NN}}$ = 200 GeV*, *Phys. Rev.* **C 77** (2008) 024912.

[15] R.V. Gavai *et al.*, *Quarkonium production in hadronic collisions*, *Int. J. Mod. Phys.* **A 10** (1995) 3043.

[16] V. Barger, W.Y. Keung and R.N. Philips, *Hadroproduction of J/ψ and Υ*, *Z. Physik* **C 6** (1980) 169, and *On J/ψ and Υ Production via Gluons*, *Phys. Lett.* **B 91** (1980) 253; R. Vogt, *J/ψ production and suppression*, *Phys. Rept.* **310** (1999) 197.

[17] V. Emel'yanov, A. Khodinov, S.R. Klein and R. Vogt, *Impact parameter dependence of J/ψ and Drell-Yan production in heavy ion collisions at $\sqrt{s_{NN}}$ = 17.3 GeV*, *Phys. Rev.* **C 59** (1999) 1860.

[18] A.D. Martin *et al.*, *MRST2001: Partons and α_s from precise deep inelastic scattering and Tevatron jet data*, *Eur. Phys. J.* **C 23** (2002) 73.

[19] J. Pumplin *et al.*, *New Generation of Parton Distributions with Uncertainties*

from Global QCD Analysis, J. High Energy Phys. **07** (2002) 012.

[20] K.J. Eskola, H. Paukkunen and C. Salgado, *An Improved global analysis of nuclear parton distribution functions including RHIC data, J. High Energy Phys.* **07** (2008) 102.

[21] K.J. Eskola, V.J. Kolhinen and C. Salgado, *The scale dependent nuclear effects in parton distributions for practical applications, Eur. Phys. J.* **C 9** (1999) 61.

[22] D. de Florian and R. Sassot, *Nuclear parton distributions at next-to-leading order, Phys. Rev.* **D 69** (2004) 074028.

[23] M. Hirai, S. Kumano and T.-H. Nagai, *Determination of nuclear parton distribution functions and their uncertainties in next-to-leading order, Phys. Rev.* **C 76** (2007) 065207.

[24] C. Lourenço and H.K. Wöhri, *Heavy flavour hadro-production from fixed-target to collider energies, Phys. Rept.* **433** (2006) 127.

[25] K.J. Eskola, V.J. Kolhinen and R. Vogt, *Enhancement of charm quark production due to nonlinear corrections to the DGLAP equations Phys. Lett.* **B 582** (2004) 157.

[26] D. Kharzeev, C. Lourenço, M. Nardi and H. Satz, *A Quantitative analysis of charmonium suppression in nuclear collisions, Z. Physik* **C 74** (1997) 307.

[27] C.W. De Jager *et al., Nuclear charge- and magnetization-density-distribution parameters from elastic electron scattering*, Atomic Data and Nuclear Data Tables **14** (1974) 479.
H. De Vries *et al., Nuclear charge-density-distribution parameters from elastic electron scattering*, Atomic Data and Nuclear Data Tables **36** (1987) 495.

[28] P. Faccioli for the HERA-B Coll., *Update on HERA-B Results*, Int. Workshop on Heavy Quarkonium, DESY, Hamburg, October 2007.
I. Abt *et al.* (HERA-B Coll.), *Kinematic distributions and nuclear effects of J/ψ production in 920 GeV fixed-target proton-nucleus collisions*, [arXiv:0812.0734].

[29] Ph. Charpentier, private communication and PhD thesis, *Etude de la production hadronique des résonances J/ψ et Upsilon de 150 à 290 GeV/c*, Universit Paris-Sud, April 1983.

[30] G. Borges *et al.* (NA50 Coll.), *The J/ψ normal nuclear absorption*, Eur. Phys. J. C **43** (2005) 161.

[31] P. Faccioli, C. Lourenço, J. Seixas and H.K. Wöhri, *Study of ψ' and χ_c decays as feed-down sources of J/ψ hadro-production, J. High Energy Phys.* **10** (2008) 004.

[32] M. Gluck, E. Reya and A. Vogt, *Dynamical parton distributions revisited, Eur. Phys. J.* **C 5** (1998) 461.

[33] H. Santos, PhD thesis, *J/ψ and ψ' Production in Pb-Pb Collisions at 158 GeV/nucleon*, Universidade Técnica de Lisboa, 2004, `http://cern.ch/NA50/theses.html`